Title: Restructuring of amygdala subregion apportion across adolescence

Abbreviated Title: Amygdala subnuclei development across adolescence

Authors: *Claire E. Campbell, BS[1], Adam F. Mezher, BS[1,2], Sandrah P. Eckel, PhD[1], J. Michael Tyszka, PhD[3], Wolfgang M. Pauli, PhD[3], Bonnie J. Nagel, PhD[4], & Megan M. Herting, PhD[1]*

Affiliations:

[1]Department of Preventive Medicine, Keck School of Medicine of University of Southern California, Los Angeles, California, USA 90033

[2]Neuroscience Graduate Program, University of Southern California, Los Angeles, California, USA 90089-2520

[3]Division of Humanities and Social Sciences, California Institute of Technology, Pasadena, California, USA 91125

[4]Departments of Psychiatry & Behavioral Neuroscience, Oregon Health & Science University, Portland, Oregon, USA 97239-3098

Corresponding Author: Megan M. Herting, PhD, Keck School of Medicine of University of Southern California, Departments of Preventive Medicine, 2001 N. Soto**,** Los Angeles, CA 90089

Number of pages: 30

Number of figures: 4

Number of tables: 6

Number of words for Abstract: 236

Number of words for Introduction: 647

Number of words for Discussion: 1478

Conflict of Interest: The authors have no conflicts of interest to disclose.

Acknowledgements: The research above was supported by the following grants, R01 AA017664 (PI: Nagel), R21 MH099618 (PI: Nagel), R03 HD090308 (PI: Herting), K01 MH108761 (PI: Herting), and NIMH P50 MH094258 (PI: Adolphs). We also thank the families who contributed their time and participated in the above study.

Abstract

Total amygdala volumes continue to increase from childhood to young adulthood. Interestingly, postmortem studies have found postnatal neuron numbers increase in a nuclei specific fashion across development, suggesting amygdala maturation may involve changes to its composition. Thus, the goal of this study was to examine amygdala subregion apportionment *in vivo* and examine if these patterns were associated with age, sex, body mass index (BMI), and pubertal status in a large sample of typically developing adolescents (N=421, 44% female, ages 10-17 years). We utilized the CIT168 atlas to examine the relative volume fraction (RVF) of 9 subregions within each hemisphere of the amygdala. Generalized Additive Mixed Models (GAMM) were used to assess how demographic variables (e.g. age, sex) and physical development (e.g. BMI and pubertal status) were associated with amygdala RVFs. Results showed that age associations varied significantly by sex for the RVFs of the lateral (LA), basolateral ventral and paralaminar subdivision (BLVPL), central nucleus (CEN), and amygdala transition areas (ATA). While pubertal development was found to be associated with RVFs in the BLVPL, CEN, and ATA in males, best-fit model comparisons revealed that age was the best predictor of relative volumes of these subregions. These results suggest that the relative apportionment of the amygdala further develops with age in males across adolescence. These findings may help elucidate how sex differences could impact the prevalence of mental health disorders that arise during this adolescent period of development.

Significance Statement: Given the heterogeneity of cytoarchitecture, connectivity, and function between amygdala subregions, naturally more research is needed to understand amygdala composition across human adolescence. Our findings show that males, but not females, demonstrate amygdala composition development across the adolescent years of 10 to 17. In males, there is a relative expansion of the lateral and central subregions, but a contraction of the basolateral ventral and paralaminar subdivision and amygdala transition areas within the amygdala. Distinct maturation patterns of the amygdaloid complex across adolescence may be an important mechanism contributing to sex differences in emotional processing as well as the onset, prevalence, and symptomatology for affective disorders that typically emerge during this developmental period.

Introduction

The amygdala is a collection of nuclei located in the temporal lobe, with extensive connections to the cerebral cortex (Amaral and Price, 1984; Barbas and De Olmos, 1990; Ghashghaei and Barbas, 2002). The heterogeneous structure and function of the amygdala nuclei play a vital role in mediating a number of cognitive, affective, and motivational processes (Baxter and Murray, 2002; Hariri et al., 2002; Meyer-Lindenberg et al., 2005; Raznahan et al., 2011; Bzdok et al., 2013; Tottenham and Gabard-Durnam, 2017). Cytoarchitecture and lesion studies have helped determine how these diverse groupings of amygdala neurons mediate specific processes (Krettek and Price, 1978; Amaral and Price, 1984; Ghashghaei and Barbas, 2002; Amunts et al., 2005; Solano-Castiella et al., 2011). Previous studies have shown the basal and lateral nuclei process high-level sensory input and emotional regulation (Sananes and Davis, 1992; Wan and Swerdlow, 1997; Schoenbaum et al., 1999), while the central and basolateral nuclei are involved in reward learning and food intake (Killcross et al., 1997; Rollins and King, 2000; Baxter and Murray, 2002; Ambroggi et al., 2008). Moreover, the region closest to the ventral horn, known as the paralaminar nucleus contains neurons that continue to mature and migrate into adulthood (Amaral and Price, 1984; Bernier et al., 2002; Tosevski et al., 2002; deCampo and Fudge, 2012); this region's potential for regional neural plasticity (deCampo and Fudge, 2012) may be important for modulating amygdala apportionment.

When treating the amygdala as a singular unit, total amygdala volumes continue to increase from childhood to young adulthood, with distinct developmental patterns seen based on sex and pubertal stage (Giedd et al., 1996; Bramen et al., 2011; Herting et al., 2014; Wierenga et al., 2014; Herting et al., 2018; Wierenga et al., 2018). However, a recent postmortem study (N=24 neurotypical brains, ages 2-48 years) found that neuron numbers increase in the amygdala, but do so in a nucleus specific manner (Avino et al., 2018). These findings suggest that neuronal increase in specific nuclei may prompt relative changes in amygdala nuclei apportionment with

development. Accordingly, our study aimed to test the hypothesis that the relative ratio of individual nuclei to the total amygdala volume, or the *relative volume fraction (RVF)*, develops across human adolescence. While previous atlases utilized *ex vivo* brain tissue to delineate the amygdala into smaller regions of interests (ROIs) (Amunts et al., 2005; Saygin et al., 2017), we implemented a novel high-resolution probabilistic atlas, known as the CIT168, based on *in vivo* MRI data (Tyszka and Pauli, 2016; Pauli et al., 2018). Using this approach, we segmented the amygdala into 9 distinct bilateral ROIs for 421 adolescents (n=186 females, ages 10-17 years), including the lateral nucleus (LA), basolateral dorsal and intermediate subdivision (BLDI), basolateral ventral and paralaminar subdivision (BLVPL), basomedial nucleus (BM), cortical and medial nuclei (CMN), central nucleus (CEN), anterior amygdala area (AAA), amygdala transition areas (ATA), and amygdalostriatal transition area (ASTA) (**Table 1**).

Choosing predictors based on previous research (Rollins and King, 2000; Baxter and Murray, 2002; Herting et al., 2014; Wierenga et al., 2014; Janak and Tye, 2015; Tyszka and Pauli, 2016; Herting et al., 2018; Wierenga et al., 2018), we explored how age, sex, body mass index (BMI), and pubertal status were associated with amygdala composition in adolescents. Given that the basolateral nucleus increases innervation with the prefrontal cortex during adolescent neurodevelopment (Cunningham et al., 2002) and the paralaminar's potential for postnatal neuroplasticity (deCampo and Fudge, 2012), we hypothesized that lateral, basal, and paralaminar subregions would be larger with age across adolescence. We also hypothesized that a higher BMI would correlate with the central and basal subregions, given their involvement in reward learning (Killcross et al., 1997; Rollins and King, 2000; Baxter and Murray, 2002; Ambroggi et al., 2008). Ultimately, understanding how the human amygdala develops throughout adolescence may help discern developmental changes seen in social-emotional and reward-related behavior, as well as identify risk factors for mental health disorders.

Materials and Methods

Participants and Measures

This study incorporated cross-sectional data from 421 adolescents (n=186 females), ages 10 to 17 years, from ongoing research studies at Oregon Health & Science University. A comprehensive telephone interview was conducted to determine eligibility for all participants, and written consent and assent were obtained from each participating adolescent and at least one of their biological parents. All participants were right-handed and free of neurological, neurodevelopmental, and/or psychological diagnoses. Detailed exclusionary criteria can be found elsewhere (Alarcon et al., 2015; Scheuer et al., 2017; Morales et al., 2018).

Based on prior research (Rollins and King, 2000; Baxter and Murray, 2002; Herting et al., 2014; Wierenga et al., 2014; Janak and Tye, 2015; Tyszka and Pauli, 2016; Herting et al., 2018; Wierenga et al., 2018), we considered four primary biological and physical factors for each participant: age, sex, pubertal status, and BMI. Pubertal status was determined by self-report using the Pubertal Development Scale (PDS) (Petersen et al., 1988), with scores for each of the 5 questions ranging from 1 (not started) to 4 (development seems complete). Scores across the items were averaged to a single comprehensive score. Weight and height were also obtained on-site within 1-week of the scan session. BMI was calculated using the Centers for Disease Control and Prevention's BMI Percentile Calculator for Child and Teen English Version (http://nccd.cdc.gov/dnpabmi/Calculator.aspx) by providing participant birth date, date of measurement, sex, height (to nearest 0.1 cm) and weight (to nearest 0.1 kg). BMI z-scores (BMIz), which correspond to growth chart percentiles, were then calculated to reflect the relative weight of the individual using the appropriate reference standard based on the individual's age and sex (Must and Anderson, 2006).

MRI Data Collection and Preprocessing

A whole-brain T1-weighted MRI scan was acquired for each participant on the same 3 Tesla MRI system (Magnetom Tim Trio, Siemens Medical Solutions, Erlangen, Germany) using a 12-channel head coil at the Oregon Health & Science University's Advanced Imaging Research Center (TR = 2300ms, TE = 3.58ms, TI = 900ms, flip angle = 10º, 256x240 matrix, voxel size = 1 mm x 1 mm x 1.1 mm). Raw images were quality checked for motion and given a rating of 1 (pass), 2 (review), or 3 (fail) (Backhausen et al., 2016). Using the Functional Magnetic Resonance Imaging of the Brain Software Library (FSL) version 5.0 (Smith et al., 2004; Woolrich et al., 2009; Jenkinson et al., 2012), each brain image was first reoriented to standard orientation using FSL's *fslreorient2std* function. Images were then automatically cropped to reduce lower head and neck using FSL's *robustfov* tool and rigid-body AC-PC aligned. Using the *antsBrainExtraction* function from the Advanced Normalization Tools (ANTs, Version 2.1.0.post691-g9bc18)(Avants et al., 2011), each image was skull-stripped to allow for an N4 Bias Field Correction (Tustison et al., 2010) on the whole-brain image.

Amygdala Segmentation

Details of the *in vivo* amygdala probabilistic atlas construction, validation, estimates of individual differences, and comparison with previous atlas' have been previously published (Tyszka and Pauli, 2016; Pauli et al., 2018). Each participant's image was registered to the CIT168 atlas using a B-spline bivariate symmetric normalization (SyN) diffeomorphic registration algorithm from ANTs (Avants et al., 2007). Implementation of the inverse diffeomorphism resulted in a probabilistic segmentation of each participant's left and right total amygdala estimates, as well as the following 9 bilateral regions of interest (ROI): lateral nucleus (LA); dorsal and intermediate divisions of the basolateral nucleus (BLDI); ventral division of the basolateral nucleus and paralaminar nucleus (BLVPL); basomedial nucleus (BM); central nucleus (CEN); cortical and medial nuclei (CMN); amygdala transition areas (ATA); amygdalostriatal transition area (ASTA); and anterior amygdala area (AAA). A 2-Dimensional visual representation of the amygdala

subregion segmentation on a representative subject can be seen in **Figure 1**. To fully demonstrate the CIT168 segmentation, overlay images of coronal slices through the entire rostral-caudal extent of the amygdala for four subjects are presented in **Figure 2**, with boundary outlines (without an overlay) presented in **Figure 2-1**. The subjects were randomly chosen to cover the distributions of our age range, including 1 male and 1 female from both the early and older adolescent periods. Descriptions of each subregion can be found in **Table 1.** A relative volume fraction (i.e. a proportion estimate) was computed for each ROI by normalizing it to the respective total amygdala volume in each hemisphere $(Relative\ Volume\ Fraction = ROI\ probabilistic\ volume/total\ amygdala\ probabilistic\ volume)$. The quality of all amygdala segmentations was confirmed visually (A.F.M.).

Contrast-to-Noise Ratio (CNR) Calculations for Segmentation Accuracy

In the creation and validation of the CIT168 atlas, Tyszka and Pauli (2016) establish that a CNR >1 provides a robust volume estimation of the ground truth volumes of an estimate. Thus, the intensity contrast within each hemisphere of the amygdala was estimated from the interquartile range of intensities within the entire amygdala from each subject's T1-weighted image. The standard deviation (SD) of the noise was estimated from the residual signal obtained from the subtracted T1-weighted atlas template image from each subject's T1-weighted image. The interquartile range (IQR) was then divided by the mean residual noise SD to generate the CNR for each individual.

Statistical Analysis

Data were analyzed in R (version 3.5.1). Linear regressions (M1) were utilized to examine the associations between age and intracranial volume (ICV), ICV and BMIz, BMIz and age, BMIz and PDS, PDS and ICV. These associations were assessed across all participants and between males and females to see if the associations were significantly different by sex:

$$M1: \quad Y = \beta_0 + \beta_1 X_1 + \beta_2 Male + \beta_3 X_1 \times Male + \varepsilon$$

To examine if total amygdala and amygdala nuclei volume composition (i.e. RVFs) related to age, sex, BMIz, and pubertal status, we employed a Generalized Additive Mixed Model (GAMM) implemented by the *mgcv* package (version 1.8-24 in R version 3.5.1, R Core Team, 2018). Given that this developmental period shows non-linear subcortical brain volume growth patterns (Wierenga et al., 2014; Herting et al., 2018), a GAMM approach was chosen as it allows for data-driven estimation of non-linear associations (with linearity as a special case), using 'smooth' functions, s(), in place of linear terms. To examine the association between age and amygdala nuclei composition, as well as determine if these associations vary by sex, RVF of each amygdala subregion was modeled independently using a GAMM (M2) with fixed effects including smooth terms for age and age-by-sex (s_1 and s_2, respectively), as well as a linear term for sex, hemisphere, BMIz, ICV, and a random intercept (U_i) for participant *i*:

$$M2: RVF_{ij} = \beta_0 + s_1(Age_i) + \beta_1 Male_i + s_2(Age_i) \times Male_i + \beta_2 Hemisphere_{ij} + \beta_3 BMIz_i + \beta_4 ICV_i + U_i + \varepsilon_{ij}$$

where $\mathrm{RVF}_{i,j}$ is the relative volume fraction (RVF) defined for each subject, i, in either the left or right hemisphere, j. Each smooth term is a shrinkage version of a cubic regression spline with four equally spaced knots.

Given that markers of pubertal development have been shown to relate to total amygdala volumes across adolescence (Goddings et al., 2014; Herting et al., 2014; Wierenga et al., 2018), we then utilized a model building strategy to determine if age, pubertal development, or their combination best predicted amygdala subregion RVFs across adolescence. Given that pubertal development follows a different age-related trajectory in males versus females and physical changes are distinct in males (e.g. facial hair, testes development) and females (e.g. breast development, menstruation) (Berenbaum et al., 2015), these analyses were performed in each

sex separately. First, in each sex we examined the smooth effect of age (M3). Next, we examined the smooth effect of pubertal stage (M4). Lastly, we examined both the smooth effects of age and pubertal stage as well as the interaction term of age-by-pubertal stage (M5), with smooths implemented by tensor product interactions, allowing for main effects and the interaction. Each model also included the fixed effects of BMIz, hemisphere, ICV, and a random intercept (U_i) for participant *i*.

$$M3: RVF_{ij} = \beta_0 + s_1(Age_i) + \beta_2 Hemisphere_{ij} + \beta_3 BMIz_i + \beta_4 ICV_i + U_i + \varepsilon_{ij}$$

$$M4: RVF_{ij} = \beta_0 + s_1(Pubertal\ Stage_i) + \beta_2 Hemisphere_{ij} + \beta_3 BMIz_i + \beta_4 ICV_i + U_i + \varepsilon_{ij}$$

$$M5: RVF_{ij} = \beta_0 + s_1(Age_i) + s_2(Pubertal\ Stage_i) + s_3(Age_i, Pubertal\ Stage_i) + \beta_2 Hemisphere_{ij} + \beta_3 BMIz_i + \beta_4 ICV_i + U_i + \varepsilon_{ij}$$

Akaike Information Criterion (AIC) and Likelihood ratio tests ($p < 0.05$) were used to compare model fits. To reduce type I error, each set of models across the 9 ROIs were corrected for multiple comparisons using the Bonferroni correction method (Bonferroni, 1936), with p-values <0.0056 deemed significant.

Results

Males and females did not differ in age, BMI, or pubertal status (PDS), though on average, males had a significantly larger ICV compared to females (β=121231, p=<0.0001) (**Table 2A**). No significant associations were detected between age and ICV, ICV and BMIz, BMIz and age, and PDS and ICV across all participants (**Table 2B**). A larger BMIz score was associated with a smaller ICV in males (p=0.04), whereas larger BMIz was associated with higher PDS scores in females (p=0.002). The associations between these variables did not significantly differ between the sexes (p's>0.05) (**Table 2B**). The mean SD of residual signal obtained from the CIT168 mask and the T1-weighted image of the whole amygdala was 24 for the right and left hemispheres. The mean lower and upper quartile intensities within the amygdala were 276 and 309 (IQR=33) for

229 the right hemisphere and 275 and 308 (IQR=33) for the left hemisphere, with the residual noise
230 standard deviations of 0.20 for both hemispheres. Therefore, the average CNR was 1.4 for the
231 amygdala in both hemispheres in our sample, suggesting the current study has sufficient CNR
232 necessary to implement reliable estimates utilizing the diffeomorphic approach (Tyszka and Pauli,
233 2016).

234 Age and sex differences in amygdala composition

235 RVFs of each subregion using the CIT168 are summarized by hemisphere and sex in
236 **Figure 3** and **Table 3**. From largest to smallest, subregion absolute volumes were on average
237 332-391 mm^3 for the lateral nucleus (~20-21% of amygdala volume); 198-to 230 mm^3 for the BLDI
238 (~12-13% of amygdala volume); 171-195 mm^3 for the CMN (~11% of the amygdala volume); 118-
239 141 mm^3 for the BLVPL (~7-8% of the amygdala volume); 114 to 131 mm^3 for the BM (~7% of the
240 amygdala volume); 93-111 mm^3 for the ATA (~5-6% of the amygdala volume); 69-77 mm^3 for the
241 ASTA (~4 % of the amygdala volume); 63-71 mm^3 for the AAA (~3-4% of the amygdala volume);
242 47-53 mm^3 for the CEN (~3% of the amygdala volume).

243 GAMM model results examining the associations between amygdala subregion RVF and
244 age, sex, hemisphere, BMIz, ICV, and age-by-sex interactions are presented in **Table 4**. A
245 significant age-by-sex interaction was detected for the LA (Adj R^2=.06), BLVPL (Adj R^2=.13), CEN
246 (Adj R^2=.10), and ATA (Adj R^2=.12) (**Figure 4**). The LA and CEN show a relative increase of the
247 total amygdala volume (as indexed by larger RVF values) with age in males, whereas females
248 show no changes in the relative volume of these amygdala subregions with age. In contrast, the
249 BLVPL and ATA show a relative decrease in relation to the total amygdala volume (e.g. smaller
250 RVFs) with age in males, whereas again no relationship is seen in females. The relative volumes
251 of the BLDI, BM, CMN, and AAA did not relate to age, sex, or their interaction. In addition, no
252 significant relationships were seen between any of the 9 subregions and BMIz.
253

Pubertal development and amygdala composition in males and females

GAMM model outputs for age (M3), puberty (M4), and age-by-puberty (M5) for each RVF in each sex separately are presented in **Table 5** for males and **Table 6** for females. For females, no significant age, puberty, or age-by-puberty associations were seen for any of the 9 amygdala subregions. In males, age was again found to be significantly associated with RVFs of the BLVPL, CEN, and ATA (M3: p's $\leq$ 0.005), and trending for LA (M3: p's $\leq$ 0.01). In addition, puberty was found to significantly relate to RVFs of the BLVPL, CEN, and ATA (M4: p's $\leq$ 0.005). There were no age-by-pubertal interactions that were significant for any of the 9 amygdala subregions after correcting for multiple comparisons; though a trend was seen for the BLVPL (age-by-PDS: p=0.05; Adj R^2: 0.14). For the BLVPL and ATA, best-fit model comparisons showed that the age and puberty model was significantly better than the model including only puberty (M4 vs. M5: p's>0.05); however, the age and puberty model was not a significantly better model than age alone (M3 vs. M5: p's>0.05).

Discussion

The current cross-sectional study provides the first glimpse at amygdala nuclei volume apportionment in adolescents. While previous studies have examined developmental changes in the total amygdala volume across childhood and adolescence (Herting et al., 2018; Wierenga et al., 2018), the current study highlights the utility of the CIT168 to define 9 amygdala subregions in a large sample of adolescents and suggests that amygdala composition may continue to modify across the adolescent period in relation to sex. Using the newly derived *in vivo* CIT168 atlas, relative changes in the subregion composition of the amygdala were associated with age in males, but not females. In males, findings suggest an expansion in relative volumes of the LA and CEN, but contraction of the BLVPL and ATA subregions, accounting for between 6 to 13% of the variance in the relative composition of these regions within the amygdala.

Our findings support the hypothesis that relative volumes occupied by nuclei within the amygdala may undergo structural reformation during the adolescent years, although only in males. While MRI and the CIT168 atlas cannot decipher each of the exact 13 nuclei of the human amygdala, our findings in males are supported by the recent histology study showing that postnatal neuron numbers change in distinct nuclei, including the central, lateral, and basal nuclei, from childhood to adulthood (Avino et al., 2018). In that study, however, a sex-specific effect was not examined, as the wide age range (n=24, 2 to 48 years) neurotypical sample had very few females (n = 5) (Avino et al., 2018). Beyond nucleus-specific changes in neuron number, postnatal immunohistochemistry studies have also found a difference in immature and mature neuron concentrations among amygdala nuclei, including the lateral, central, basal, and paralaminar nucleus (Avino et al., 2018). A higher concentration of immature neurons has been reported in the paralaminar nucleus (part of the BLVPL subregion in the current study) as compared to other amygdala nuclei (Avino et al., 2018). Moreover, the number of immature neurons in the paralaminar nucleus decreases over time, whereas the mature neuron numbers of the surrounding regions continue to increase in childhood and adolescence. These data have led to the hypothesis that gradual maturation and migration of paralaminar immature neurons may contribute to the mature neuron number within the paralaminar, and/or be the source of increases in neuron number seen in other nuclei over development. If this hypothesis proves to be correct, migration and maturation of immature neurons may contribute to the re-configuration and/or refinement of the amygdala subregions and their subsequent connectivity with the cerebral cortex across adolescence. While MRI cannot assess neuron number, more research is needed to determine if decreases in the relative fraction of the BLVPL and ATA but increases in the surround LA and CEN in males may be suggestive of distinct nuclei maturation and migration patterns in amygdala development. Combining postmortem histology and MRI segmentation approaches in

302 developing samples is necessary to further decipher if these age and sex-specific patterns occur
303 across development.

304 Furthermore, cytoarchitectural findings suggest the BLVPL of the amygdala receives
305 afferents from both the lateral nucleus (LA) and the hippocampus (Pitkanen and Amaral, 1998).
306 Efferents of the medial paralaminar nucleus gradually merge with the periamygdaloid cortex, often
307 termed the “corticoamygdaloid transition area”, which further projects to the hippocampus.
308 Moreover, the lateral nucleus (LA) receives sensory information, allowing the basolateral complex
309 to process the information, and then send this information out of the amygdala via the central
310 nucleus (CEN) (McDonald and Jackson, 1987; Sah et al., 2003). The CIT168 ATA region
311 encapsulates the periamygdaloid cortex, as well as these amygdalocortical and
312 amygdolohippocampal transition areas. Hippocampal input to the amygdala is important for
313 contextual fear learning (Phillips and LeDoux, 1992), and given the convergence between sensory
314 input from the LA, as well as bidirectional connectivity with the hippocampus, it has been proposed
315 that the paralaminar and periamygdaloid cortex of the amygdala may be involved in contextual
316 learning (deCampo and Fudge, 2013). It remains to be elucidated how age expansion for the LA,
317 CEN, but contraction for the BLVPL and ATA, in males may map onto function. However,
318 amygdala nuclei composition may be an additional MRI feature to explore in hopes of clarifying
319 our understanding of amygdala structural and functional development. It may also prove useful in
320 studying known sex differences in emotion-related behavior, brain function, and prevalence in
321 mental health disorders that typically emerge during this time. For example, meta-analysis of 166
322 studies found a small, yet consistent, sex difference in positive and negative emotional expression
323 that begins to diverge in the beginning of childhood and into adolescence (Chaplin and Aldao,
324 2013). Similarly, fMRI studies have reported greater brain activity in cortical regions, including
325 visual and parietal regions, in male versus female adolescents during emotional functional MRI
326 tasks (Cservenka et al., 2015). Resting-state fMRI studies implementing *ex vivo* atlases to define

basolateral, superficial, and centromedial subregions, have also found age and sex-specific differences in amygdala functional connectivity patterns. Age and region-specific patterns were seen between the amygdala and medial prefrontal cortex, with connectivity becoming apparent at age 10 and continuing to strengthen across adolescence (GabardDurnam et al., 2014). In a separate study, the superficial amygdala resting-state patterns were found to be more mature in female adolescents, but basolateral amygdala connectivity patterns were more mature in male adolescents (Alarcon et al., 2015). Future studies are warranted to determine if the relative expansion of the primary input (LA) and output (CEN) subregions, but contraction of contextual and emotional learning subregions (BLVPL, ATA) in males, may relate to differences in emotional expression, greater cortical activation to emotional stimuli and/or stronger basolateral functional connectivity in males versus females during adolescence. Beyond the possible functional implications of nuclei apportionment, implementation of the CIT168 atlas to construct ROIs for other MRI modalities, including resting-state fMRI, task-based fMRI, and diffusion, may also assist in gaining greater specificity of how different amygdala nuclei functionally and structurally develop.

While this is the first study to examine amygdala nuclei volume composition in adolescents, the current study has both strengths and limitations. Other amygdala segmentation approaches are derived from post-mortem samples that are largely based on smaller samples of older male brains (Amunts et al., 2005; Saygin et al., 2017), which not only fail to capture possible developmental changes but may also be confounded by factors that influence tissue quality (Stan et al., 2006). The CIT168 atlas mitigates some of these concerns by using the high-resolution (700 micrometer) *in vivo* Human Connectome Project data from young adults (ages 22-35 years). Furthermore, the current study illustrates the ability to apply this newly developed CIT168 atlas to assess 9 distinct amygdala subregions in adolescents, given our similar total probabilistic and relative amygdala volumes based on our adolescent T1-weighted images and the CIT168 T1 and T2-weighted images (Tyszka and Pauli, 2016). Moreover, our hypothesis that physical growth

metrics, including body mass and pubertal development would relate to amygdala composition during adolescence was not supported. While physical characteristics of pubertal maturation did relate to BLVPL, CEN, and ATA, our current results suggest that age alone best accounts for individual differences in amygdala nuclei volume composition in males. Moreover, neither age nor pubertal status related to any of the nuclei examined in females. It is possible the lack of associations is due to our study sample. Although pubertal development scores were on average similar between the sexes in our sample (**Table 2**), there were fewer females that fell within the pre-pubertal and early pubertal range as compared to males in this age range of 10 to 17 years. While this is to be expected given the known sex difference in pubertal onset, with girls showing physical signs of maturation ~1-2 years prior to males (Dorn, 2006), more research is needed in younger females in order to assess if similar patterns of amygdala maturation do occur at slightly younger ages in females. Furthermore, it would also be helpful to utilize other markers that may be more accurate for capturing both puberty and obesity in children, such as pubertal hormone levels and measurements of body composition.

To summarize, we show the adolescent amygdala can be segmented into 9 subregions using the newly developed CIT168 atlas and that the relative composition of these amygdala subregions may continue to restructure in a sex-specific fashion during the adolescent window of development. By using this approach in conjunction with considering how the amygdala nuclei composition may continue to develop, future studies may be able to further explore how the amygdaloid complex may interact with distinct cortical regions, such as the prefrontal cortex, in order to modulate each other's development and social and emotional behaviors that continue to mature during this critical period in development (Andersen and Teicher, 2008; Tottenham and Gabard-Durnam, 2017). Our approach provides a first step towards a more rigorous exploration of functional and structural connectivity development within the heterogeneous amygdala complex across adolescence.

Figure Legends

Figure 1: Probabilistic segmentation of amygdala subregions in a representative adolescent. Structural MRI and probabilistic estimates of 9 bilateral subregions shown in the A) coronal and B) sagittal view (thresholded at probabilistic value of .3 for visualization purposes). Key: LA, lateral nucleus; BLDI, basolateral dorsal and intermediate subdivision; BLVPL, basolateral ventral and paralaminar subdivision; BM, basomedial nucleus; CMN, cortical and medial nuclei; CEN, central nucleus; AAA, anterior amygdala area; ATA, amygdala transition area; ASTA, amygdalostriatal transition area. Based on CIT168 atlas, regions of the amygdala not assigned to a specific subregion are collected into the whole AMY (other) label.

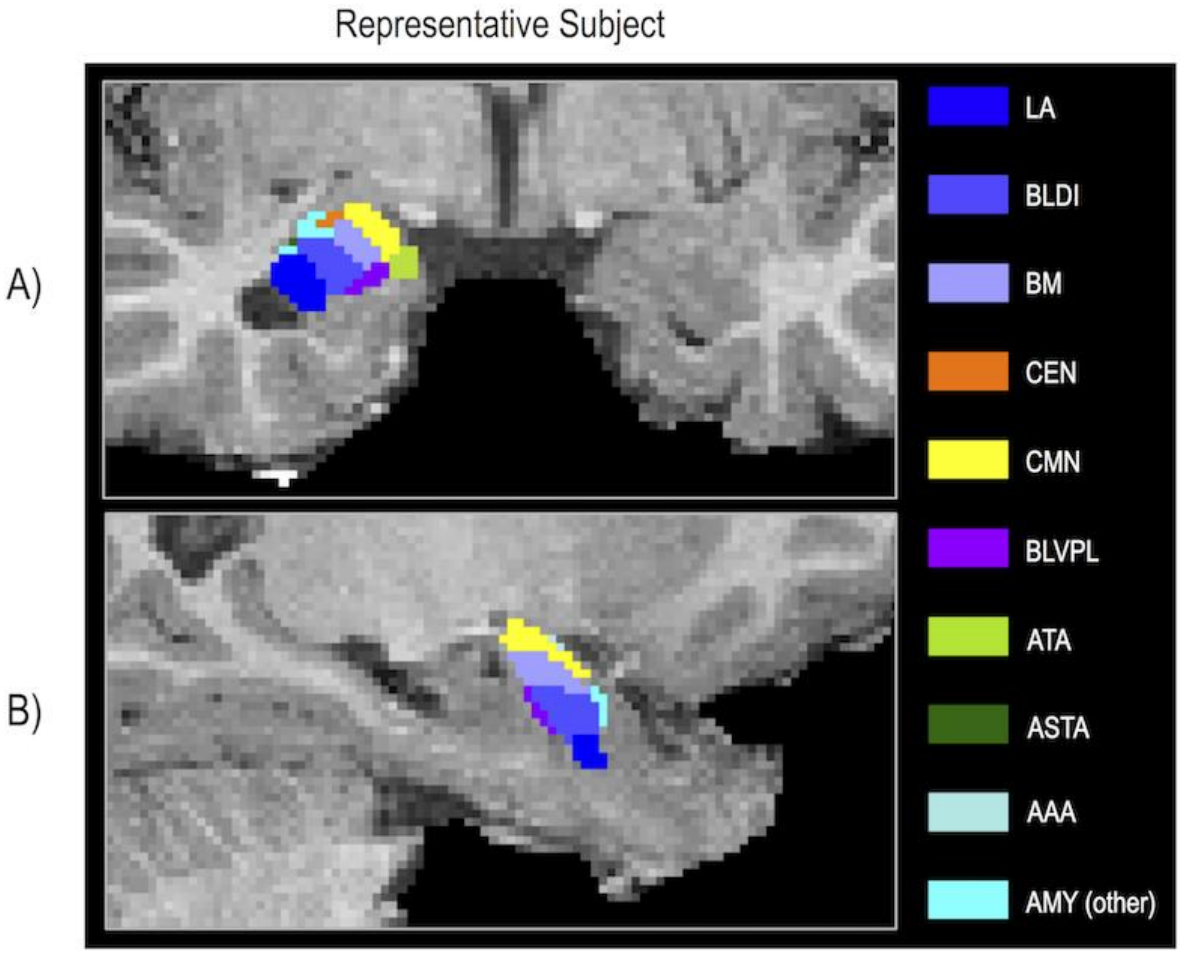

Figure 2: Overlay of CIT168 segmentation on coronal slices through entire rostral-caudal view of the amygdala in the right hemisphere for four representative subjects. A maximum likelihood label was created for each subregion of the amygdala by creating a label based on a simple competition between probabilistic labels with a thresholded probabilistic value of .3 for visualization purposes; slices (1mm) are sequential (no gap).

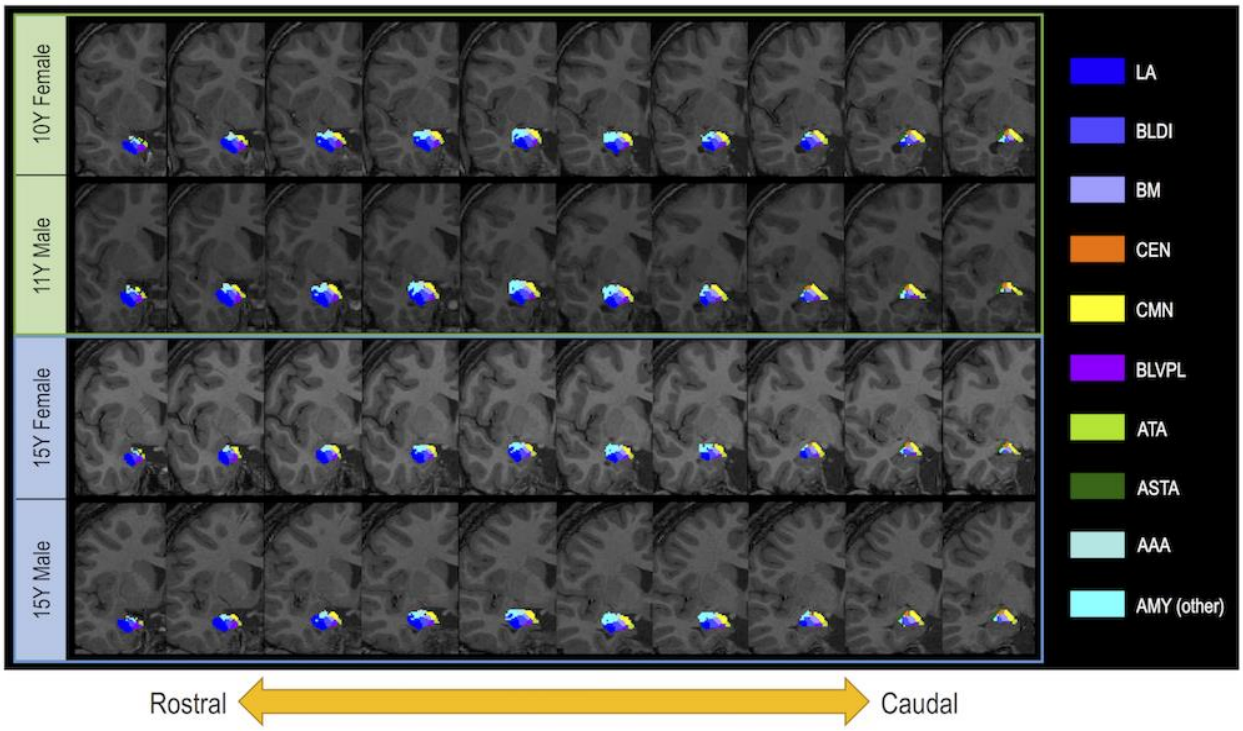

Figure 2-1: Outline of CIT168 segmentation on coronal slices through entire rostral-caudal view of the amygdala in the right hemisphere for four representative subjects. A maximum likelihood label was created for each subregion of the amygdala by creating a label based on a simple competition between probabilistic labels with a thresholded probabilistic value of .3 for visualization purposes; slices (1mm) are sequential (no gap).

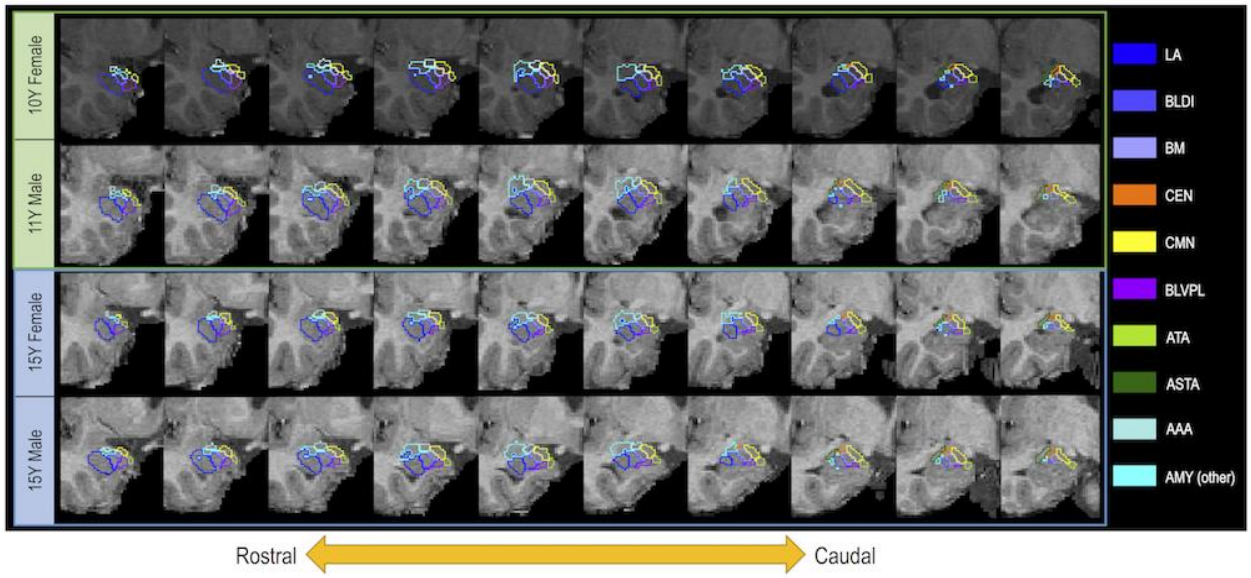

Figure 3: Amygdala subregion volumes and relative volume fractions in adolescent males and females. A) Probabilistic volumes (mm^3) and B) relative volume fraction (RVF; proportional to total amygdala volume) for each of the 9 bilateral amygdala subregion ROIs.

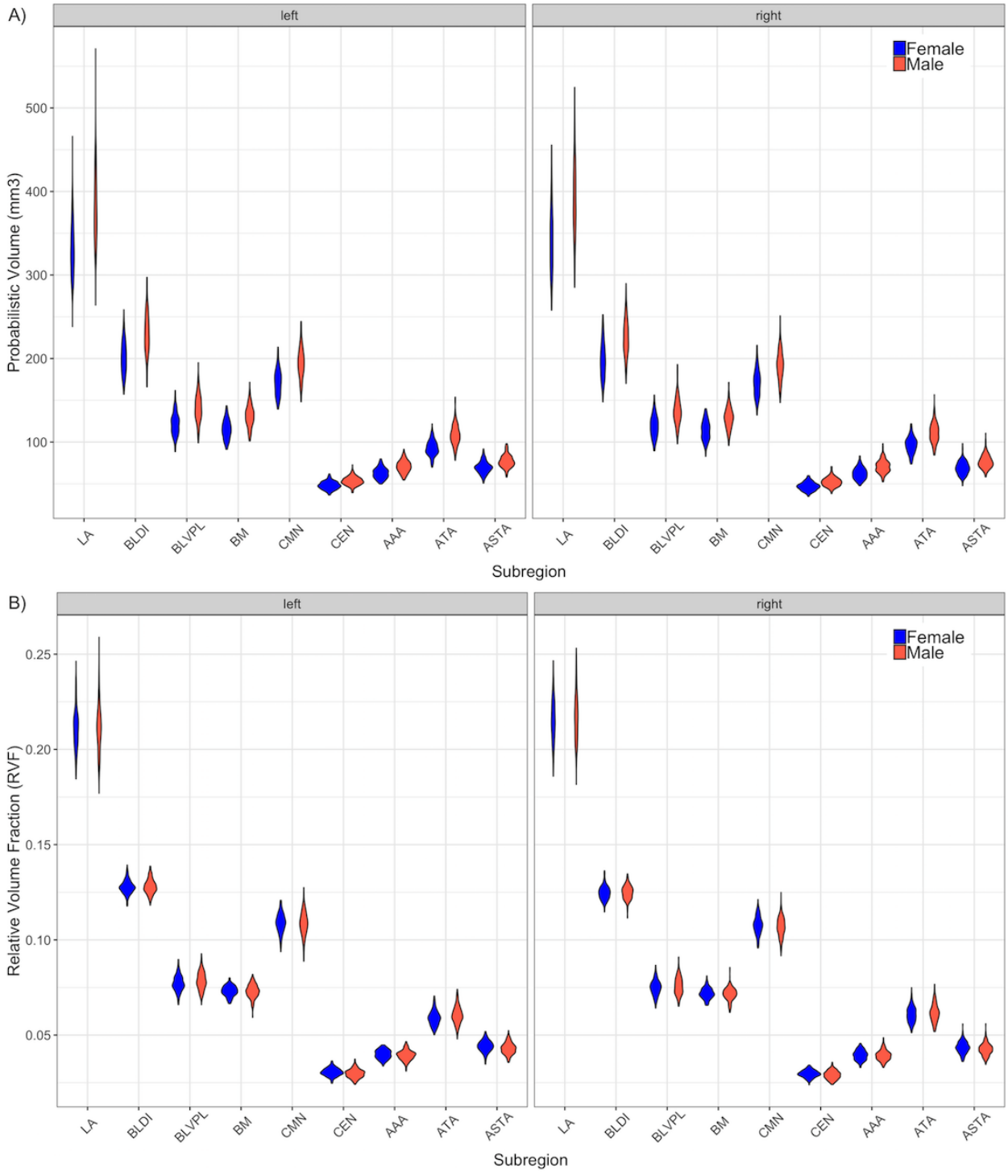

Figure 4: **Sex differences in age associations with RVF of the amygdala subregions.** A) Lateral nucleus (LA), B) Basolateral ventral and paralaminar subdivision (BLVPL) and C) Central (CEN) and D) Amygdala transition area (ATA). RVF plotted by age and sex (collapsed across hemispheres); solid lines reflect GAMM predicted fit estimates and dashed lines reflect 95% confidence intervals.

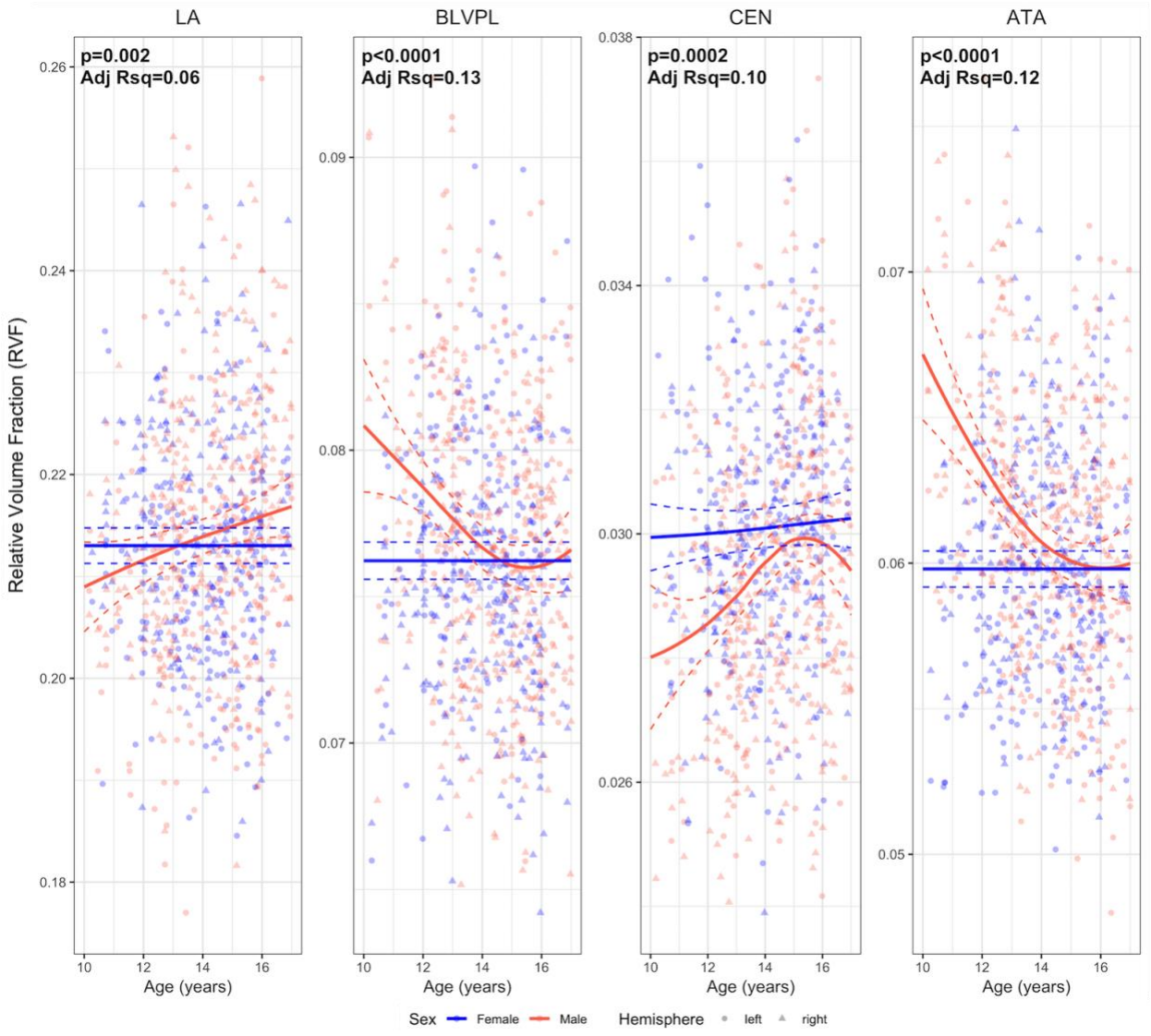

Tables

Table 1. *Amygdala Subregion ROIs*

	CIT168 Regions								
Subregion name	Lateral nucleus	Basolateral dorsal and intermediate subdivision	Basolateral ventral and paralaminar subdivision	Basomedial nucleus	Cortical and medical nuclei	Central nucleus	Anterior amygdala area	Amygdala transition area	Amygdalostriatal transition area
Subregion abbreviation	(LA)	(BLDI)	(BLVPL)	(BM)	(CMN)	(CEN)	(AAA)	(ATA)	(ASTA)
Subregion location or other common names	Surrounded ventrally and caudally by lateral ventricle, and laterally by temporal lobe white matter; primary input from neocortex	Subdivision of the basolateral nucleus; the basolateral nucleus lies medially to the lateral nucleus (LA)	Subdivision of the basolateral nucleus; the basolateral nucleus lies medially to the lateral nucleus (LA)	Ventrally bounded by BLV; BM also known as the accessory basal nucleus	Lies along dorsomedial surface of amygdaloid complex	Major output nuclei; lies dorsally and caudally within complex	Lies rostrally and caudally within complex; borders pariamygdaloid claustrum and basolateral complex	Boundary between enterhinal cortex and CMN	Lies medially and ventrally to temporal branch of anterior commissure; borders ventral putamen
Subregion content	LA exclusively	Merger between the basolateral nucleus' 2 out of 3 divisions: dorsal (BLD) and intermediate (BLI)	Merger between the basolateral nucleus' 3rd division, ventral (BLV), and the paralaminar nucleus	BM exclusively	Merger between cortical nucleus (CoA) and corticomedical group (CoMe); CoMe is made up of the internal boundaries between CoA, posterior cortical nucleus (CoP), amygdalohippocampal (AHA), nucleus of the lateral olfactory tract (NLOT), and medial nucleus (Me)	CEN exclusively	AAA exclusively	Merger between amygdalocortical and amygdalohippocampal transition areas, and periamygdaloid cortex	ASTA exclusively

Descriptions based on the CIT168 atlas by Tyszka JM, Pauli WM (2016)

Table 2. *Sample characteristics*

A) *Demographics of study participants*

	All			Female			Male			Difference between Male and Female		
	N	Mean	SD	N	Mean	SD	N	Mean	SD	*df*	Coefficient	p-value
Age	421	14.13	1.64	186	14.00	1.60	235	14.22	1.67	417	0.37	0.81
BMIz	421	0.50	0.99	186	0.47	0.92	235	0.52	1.04	417	0.42	0.49
ICV	421	1464124	139299	186	1372108	103182	235	1536954	119808	417	121231	**<0.0001**
PDS	421	2.78	0.77	186	3.06	0.72	235	2.56	0.74	417	-5.60E-02	0.93

B) *Associations between predictors*

	All			Female			Male			Difference between Male and Female		
	df	Coefficient	p-value	*df*	Coefficient	p-value	*df*	Coefficient	p-value	*df*	Coefficient	p-value
Age to ICV	417	1.5E-07	0.84	184	2.5E-07	0.83	234	5.4E-08	0.95	417	-1.4E-07	0.90
ICV to BMIz	417	-9115	0.11	184	-2855	0.73	234	-15375	**0.04**	417	-8853	0.27
BMIz to Age	417	0.03	0.39	184	0.05	0.29	234	0.0066	0.87	417	-0.03	0.52
PDS to ICV	417	1.9E-07	0.57	184	3.4E-07	0.51	234	3.2E-08	0.94	417	-2.2E-07	0.64
BMIz to PDS	417	0.19	**0.004**	184	0.29	**0.002**	234	0.09	0.33	417	-0.14	0.13

Notes: P-values with significance level of less than 0.05 are bolded. Abbreviations: SD, standard deviation, BMIz, Body Mass Index z-score; PDS, Pubertal Development Scale; ICV, Intracranial Volume

Table 3. *Probabilistic amygdala subregions by sex*

A) *Absolute probabilistic volume for each subregion (mm^3)*

		LA		BLDI		BLVPL		BM		CMN		CEN		AAA		ATA		ASTA	
Sex	Hemisphere	Mean	CoV (%)	Mean	CoV	Mean	CoV	Mean	CoV	Mean	CoV	Mean	CoV	Mean	CoV	Mean	CoV	Mean	CoV
Female	Left	332.02	9.99	201.36	9.87	121.69	10.92	115.19	9.85	171.46	9.00	48.07	9.95	62.82	10.34	92.74	9.95	69.58	10.50
	Right	341.98	11.22	198.02	10.77	118.86	11.16	114.10	10.22	170.75	9.33	46.96	10.46	62.59	11.26	96.43	10.18	68.99	11.34
Male	Left	379.68	11.51	230.04	10.22	141.22	11.75	131.21	10.08	194.80	9.38	53.36	9.71	70.71	10.23	108.64	11.23	77.07	9.79
	Right	391.12	10.97	225.56	9.81	136.82	11.44	129.08	10.23	192.52	9.32	52.26	10.47	70.88	10.85	111.04	10.67	76.56	10.46

B) *Relative volume fraction for each subregion (to total amygdala volume)*

		LA		BLDI		BLVPL		BM		CMN		CEN		AAA		ATA		ASTA	
Sex	Hemisphere	Mean	CoV (%)	Mean	CoV	Mean	CoV	Mean	CoV	Mean	CoV	Mean	CoV	Mean	CoV	Mean	CoV	Mean	CoV
Female	Left	0.21	4.89	0.13	2.75	0.08	5.46	0.07	3.75	0.11	4.63	0.03	6.84	0.04	6.02	0.06	6.58	0.04	6.74
	Right	0.22	5.27	0.12	2.84	0.07	5.32	0.07	4.00	0.11	4.49	0.03	6.32	0.04	6.63	0.06	6.80	0.04	7.23
Male	Left	0.21	5.91	0.13	3.00	0.08	6.03	0.07	4.88	0.11	5.52	0.03	7.84	0.04	6.76	0.06	7.62	0.04	7.11
	Right	0.22	5.80	0.12	2.86	0.08	6.14	0.07	4.76	0.11	4.96	0.03	7.77	0.04	7.03	0.06	7.62	0.04	7.47

Notes: Mean and coefficient of variation (CoV, mean/SD x 100%) for each subregion's probabilistic volume in millimeters cubed (mm^3) or Relative Volume Fractions (RVF) in each brain hemisphere (right and left) for both males and females. Abbreviations: See Table 1.

Table 4. *GAMM results for amygdala subregion RVF associations with age, sex, and age sex interaction, controlling for hemisphere, BMI, and ICV.*

LA						CEN					
	edf	*Ref.df*	*F*	*p-value*	Adj R squared		*edf*	*Ref.df*	*F*	*p-value*	Adj R squared
s(age)	0	3	0	1.00		s(age)	0.50	3	0.28	0.18	
s(age*sex(male))	1.26	3	2.91	***0.002***		s(age*sex(male))	2.40	3	5.02	***0.0002***	
	Estimate	*SE*	*t-value*	*p-value*			*Estimate*	*SE*	*t-value*	*p-value*	
Intercept	0.21	0.006	32.87	***<0.0001***	0.0599	Intercept	0.03	0.001	26.30	***<0.0001***	0.0964
Sex (male)	0.001	0.0009	0.74	0.46		Sex (male)	-0.001	0.0002	-3.36	***0.001***	
Hemisphere (right)	0.01	0.0006	8.88	***<0.0001***		Hemisphere (right)	-0.001	0.0001	-7.40	***<0.0001***	
BMI	0.001	0.0005	1.20	0.23		BMI	0.0001	0.0001	1.22	0.22	
ICV	0	0	-0.20	0.84		ICV	0	0	0.15	0.88	
BLDI						**AAA**					
	edf	*Ref.df*	*F*	*p-value*	Adj R squared		*edf*	*Ref.df*	*F*	*p-value*	Adj R squared
s(age)	0	3	0	0.44		s(age)	0.17	3	0.07	0.28	
s(age*sex(male))	0	3	0	0.33		s(age*sex(male))	0	3	0	0.72	
	Estimate	*SE*	*t-value*	*p-value*			*Estimate*	*SE*	*t-value*	*p-value*	
Intercept	0.13	0.002	62.88	***<0.0001***	0.1479	Intercept	0.04	0.001	31.41	***<0.0001***	0.0104
Sex (male)	0	0.0003	0.16	0.88		Sex (male)	0	0.0002	0.08	0.94	
Hemisphere (right)	-0.003	0.0002	-17.00	***<0.0001***		Hemisphere (right)	-0.0002	0.0001	-1.61	0.11	
BMI	-0.0001	0.0002	-0.88	0.38		BMI	0.0001	0.0001	0.92	0.36	
ICV	0	0	1.04	0.30		ICV	0	0	-2.17	0.03	
BLVPL						**ATA**					
	edf	*Ref.df*	*F*	*p-value*	Adj R squared		*edf*	*Ref.df*	*F*	*p-value*	Adj R squared
s(age)	0	3	0	0.71		s(age)	0	3	0	0.68	
s(age*sex(male))	2.20	3	8.71	***<0.0001***		s(age*sex(male))	2.27	3	16.37	***<0.0001***	
	Estimate	*SE*	*t-value*	*p-value*			*Estimate*	*SE*	*t-value*	*p-value*	
Intercept	0.07	0.002	32.03	***<0.0001***	0.1334	Intercept	0.06	0.002	26.78	***<0.0001***	0.1205
Sex (male)	0.001	0.0003	1.85	0.07		Sex (male)	0.001	0.0003	3.23	***0.001***	
Hemisphere (right)	-0.003	0.0002	-11.22	***<0.0001***		Hemisphere (right)	0.001	0.0002	6.80	***<0.0001***	
BMI	-0.0004	0.0002	-1.94	0.05		BMI	-0.0004	0.0002	-1.98	0.05	
ICV	0	0	1.42	0.15		ICV	0	0	-0.55	0.58	
BM						**ASTA**					
	edf	*Ref.df*	*F*	*p-value*	Adj R squared		*edf*	*Ref.df*	*F*	*p-value*	Adj R squared
s(age)	0	3	0	0.68		s(age)	0	3	0	0.50	
s(age*sex(male))	0	3	0	0.42		s(age*sex(male))	1.49	3	2.64	0.01	
	Estimate	*SE*	*t-value*	*p-value*			*Estimate*	*SE*	*t-value*	*p-value*	
Intercept	0.07	0.002	40.23	***<0.0001***	0.0565	Intercept	0.04	0.002	26.54	***<0.0001***	0.0505
Sex (male)	-0.001	0.0002	-2.27	0.02		Sex (male)	-0.001	0.0002	-3.26	***0.001***	
Hemisphere (right)	-0.001	0.0002	-8.03	***<0.0001***		Hemisphere (right)	-0.001	0.0002	-3.65	***0.0003***	
BMI	-0.0002	0.0001	-1.18	0.24		BMI	0.0002	0.0001	1.23	0.22	
ICV	0	0	2.91	***0.004***		ICV	0	0	-0.49	0.63	
CMN											
	edf	*Ref.df*	*F*	*p-value*	Adj R squared						
s(age)	0	3	0	0.53							
s(age*sex(male))	0.41	3	0.21	0.21							
	Estimate	*SE*	*t-value*	*p-value*							
Intercept	0.11	0.003	37.88	***<0.0001***	0.0216						
Sex (male)	-0.0002	0.0004	-0.50	0.62							
Hemisphere (right)	-0.002	0.0003	-5.76	***<0.0001***							
BMI	0.0001	0.0002	0.27	0.79							
ICV	0	0	-1.01	0.31							

Notes: In each model, for the parametric terms, the estimate, standard error (SE), t-value, and p-value are shown, for the smooth terms, the estimated degree of freedom (edf), reference degree of freedom (Ref.df), F-score, and p-value are shown; the Adjusted R^2 for each model is also shown. P-values of significance level less than 0.0056 bolded. Abbreviations: See Table 1.

Table 5. *GAMM amygdala subregion results for age, pubertal status, and age-by-pubertal status interaction for males*

MALES													
LA	**Smooth Terms**						**Model Fit**						
	Terms	**edf**	**Ref.df**	**F**	**p-value**	**R2**	**df**	**AIC**	**BIC**	**logLik**	**Test**	**L.Ratio**	**p-value**
M3	s(age)	1.22	3	2.42	0.006	0.0740	7	-2829.15	-2800.14	1421.57	M3 vs. M5	0.10	0.999
M4	s(pds)	0.92	3	1.45	0.023	0.0651	7	-2827.02	-2798.01	1420.51	M4 vs. M5	2.23	0.694
M5	ti(age)	0.99	3	2.01	0.009	0.0718	11	-2821.25	-2775.66	1421.62			
	ti(pds)	0.00	3	0.00	0.535								
	ti(age, pds)	1.00	1	0.12	0.734								
BLDI	**Smooth Terms**						**Model Fit**						
	Terms	**edf**	**Ref.df**	**F**	**p-value**	**R2**	**df**	**AIC**	**BIC**	**logLik**	**Test**	**L.Ratio**	**p-value**
M3	s(age)	0.05	3	0.02	0.312	0.1359	7	-3946.18	-3917.17	1980.09	M3 vs. M5	1.93	0.748
M4	s(pds)	0.77	3	0.85	0.063	0.1434	7	-3947.44	-3918.43	1980.72	M4 vs. M5	0.67	0.955
M5	ti(age)	0.00	3	0.00	1.000	0.1426	11	-3940.11	-3894.53	1981.06			
	ti(pds)	0.61	3	0.52	0.107								
	ti(age, pds)	1.00	1	0.71	0.400								
BLVPL	**Smooth Terms**						**Model Fit**						
	Terms	**edf**	**Ref.df**	**F**	**p-value**	**R2**	**df**	**AIC**	**BIC**	**logLik**	**Test**	**L.Ratio**	**p-value**
M3	s(age)	2.14	3	7.52	***<0.0001***	0.1471	7	-3749.96	-3720.96	1881.98	M3 vs. M5	2.19	0.701
M4	s(pds)	1.12	3	2.76	***0.003***	0.1093	7	-3740.20	-3711.19	1877.10	M4 vs. M5	11.95	***0.018***
M5	ti(age)	1.18	3	3.72	***0.001***	0.1427	11	-3744.16	-3698.57	1883.08			
	ti(pds)	0.00	3	0.00	0.713								
	ti(age, pds)	1.00	1	3.75	0.053								
BM	**Smooth Terms**						**Model Fit**						
	Terms	**edf**	**Ref.df**	**F**	**p-value**	**R2**	**df**	**AIC**	**BIC**	**logLik**	**Test**	**L.Ratio**	**p-value**
M3	s(age)	0.00	3	0.00	0.459	0.0607	7	-4004.17	-3975.16	2009.09	M3 vs. M5	0.28	0.991
M4	s(pds)	0.18	3	0.07	0.276	0.0615	7	-4004.19	-3975.18	2009.10	M4 vs. M5	0.26	0.992
M5	ti(age)	0.00	3	0.00	0.524	0.0640	11	-3996.46	-3950.87	2009.23			
	ti(pds)	0.00	3	0.00	0.311								
	ti(age, pds)	1.77	1.7701	0.52	0.640								
CMN	**Smooth Terms**						**Model Fit**						
	Terms	**edf**	**Ref.df**	**F**	**p-value**	**R2**	**df**	**AIC**	**BIC**	**logLik**	**Test**	**L.Ratio**	**p-value**
M3	s(age)	0.23	3	0.10	0.263	0.0204	7	-3563.78	-3534.77	1788.89	M3 vs. M5	0.01	1.000
M4	s(pds)	0.00	3	0.00	0.712	0.0192	7	-3563.75	-3534.74	1788.87	M4 vs. M5	0.02	1.000
M5	ti(age)	0.00	3	0.00	0.543	0.0385	11	-3555.77	-3510.18	1788.88			
	ti(pds)	0.00	3	0.00	0.864								
	ti(age, pds)	3.63	3.634	0.53	0.666								
CEN	**Smooth Terms**						**Model Fit**						
	Terms	**edf**	**Ref.df**	**F**	**p-value**	**R2**	**df**	**AIC**	**BIC**	**logLik**	**Test**	**L.Ratio**	**p-value**
M3	s(age)	2.31	3	6.98	***<0.0001***	0.0867	7	-4405.52	-4376.51	2209.76	M3 vs. M5	0.07	0.999
M4	s(pds)	1.05	3	2.47	***0.004***	0.0480	7	-4397.59	-4368.58	2205.79	M4 vs. M5	8.00	0.092
M5	ti(age)	2.22	3	5.90	***<0.0001***	0.0870	11	-4397.59	-4352.00	2209.79			
	ti(pds)	0.00	3	0.00	0.712								
	ti(age, pds)	1.00	1	0.09	0.762								
AAA	**Smooth Terms**						**Model Fit**						
	Terms	**edf**	**Ref.df**	**F**	**p-value**	**R2**	**df**	**AIC**	**BIC**	**logLik**	**Test**	**L.Ratio**	**p-value**
M3	s(age)	0.00	3	0.00	0.641	-0.0006	7	-4203.10	-4174.09	2108.55	M3 vs. M5	2.52	0.640
M4	s(pds)	0.00	3	0.00	0.832	-0.0006	7	-4203.10	-4174.09	2108.55	M4 vs. M5	2.52	0.640
M5	ti(age)	0.00	3	0.00	0.692	0.0203	11	-4197.62	-4152.04	2109.81			
	ti(pds)	0.00	3	0.00	0.966								
	ti(age, pds)	3.31	3.3104	1.91	0.153								
ATA	**Smooth Terms**						**Model Fit**						
	Terms	**edf**	**Ref.df**	**F**	**p-value**	**R2**	**df**	**AIC**	**BIC**	**logLik**	**Test**	**L.Ratio**	**p-value**
M3	s(age)	2.30	3	15.39	***<0.0001***	0.1599	7	-3800.48	-3771.47	1907.24	M3 vs. M5	0.00	1.000
M4	s(pds)	1.32	3	5.62	***<0.0001***	0.0863	7	-3778.35	-3749.34	1896.17	M4 vs. M5	22.13	***0.0002***
M5	ti(age)	2.11	3	10.70	***<0.0001***	0.1587	11	-3792.48	-3746.89	1907.24			
	ti(pds)	0.00	3	0.00	0.462								
	ti(age, pds)	1.00	1	0.00	0.951								
ASTA	**Smooth Terms**						**Model Fit**						
	Terms	**edf**	**Ref.df**	**F**	**p-value**	**R2**	**df**	**AIC**	**BIC**	**logLik**	**Test**	**L.Ratio**	**p-value**
M3	s(age)	1.49	3	2.67	0.006	0.0319	7	-4109.90	-4080.89	2061.95	M3 vs. M5	1.68	0.794
M4	s(pds)	0.76	3	0.79	0.072	0.0142	7	-4106.50	-4077.50	2060.25	M4 vs. M5	5.08	0.279
M5	ti(age)	0.70	3	0.70	0.064	0.0332	11	-4103.58	-4058.00	2062.79			
	ti(pds)	0.00	3	0.00	0.728								
	ti(age, pds)	1.79	1.7895	1.12	0.221								

Notes: In each model, the smooth terms, the estimated degree of freedom (edf), reference degree of freedom (Ref.df), F-score, p-value, and Adjusted R^2 for each model is shown; p-value < 0.0056 bolded (Bonferroni corrected). Between model comparisons include the df, AIC, log-likelihood ratio (L Ratio) and p-values < 0.05 bolded.

Table 6. *GAMM amygdala subregion results for age, pubertal status, and age-by-pubertal status interaction for females*

FEMALES													
LA	**Smooth Terms**						**Model Fit**						
	Terms	**edf**	**Ref.df**	**F**	**p-value**	**R2**	**df**	**AIC**	**BIC**	**logLik**	**Test**	**L.Ratio**	**p-value**
M3	s(age)	0	3	0	0.579	0.0386	7	-2325.71	-2298.32	1169.86	M3 vs. M5	0.56	0.967
M4	s(pds)	0	3	0	0.649	0.0386	7	-2325.71	-2298.32	1169.86	M4 vs. M5	0.56	0.967
M5	ti(age)	0	3	0	0.730	0.0381	11	-2318.28	-2275.23	1170.14			
	ti(pds)	0	3	0	0.910								
	ti(age, pds)	1	1	0.56	0.455								
BLDI*	**Smooth Terms**						**Model Fit**						
	Terms	**edf**	**Ref.df**	**F**	**p-value**	**R2**	**df**	**AIC**	**BIC**	**logLik**	**Test**	**L.Ratio**	**p-value**
M3	s(age)	0	3	0	1.000	0.1896	7	-3180.56	-3153.16	1597.28	M3 vs. M5	0.00	1.000
M4	s(pds)	0	3	0	1.000	0.1896	7	-3180.56	-3153.16	1597.28	M4 vs. M5	0.00	1.000
M5	ti(age)	0	4	0	1.000	0.1896	11	-3172.56	-3129.51	1597.28			
	ti(pds)	0	4	0	0.915								
	ti(age, pds)	1	1	0.002	0.966								
BLVPL	**Smooth Terms**						**Model Fit**						
	Terms	**edf**	**Ref.df**	**F**	**p-value**	**R2**	**df**	**AIC**	**BIC**	**logLik**	**Test**	**L.Ratio**	**p-value**
M3	s(age)	1.60	3	1.05	0.139	0.0883	7	-3035.01	-3007.61	1524.50	M3 vs. M5	3.16	0.532
M4	s(pds)	0	3	0	0.358	0.0766	7	-3035.76	-3008.36	1524.88	M4 vs. M5	2.41	0.662
M5	ti(age)	0	3	0	0.290	0.0877	11	-3030.17	-2987.12	1526.08			
	ti(pds)	0	3	0	1.000								
	ti(age, pds)	1.73	1.73	1.05	0.220								
BM	**Smooth Terms**						**Model Fit**						
	Terms	**edf**	**Ref.df**	**F**	**p-value**	**R2**	**df**	**AIC**	**BIC**	**logLik**	**Test**	**L.Ratio**	**p-value**
M3	s(age)	0	3	0	0.539	0.0423	7	-3302.28	-3274.88	1658.14	M3 vs. M5	1.46	0.833
M4	s(pds)	0	3	0	0.530	0.0423	7	-3302.28	-3274.88	1658.14	M4 vs. M5	1.46	0.833
M5	ti(age)	0	3	0	0.789	0.0445	11	-3295.74	-3252.69	1658.87			
	ti(pds)	0	3	0	0.969								
	ti(age, pds)	1	1	1.45	0.229								
CMN	**Smooth Terms**						**Model Fit**						
	Terms	**edf**	**Ref.df**	**F**	**p-value**	**R2**	**df**	**AIC**	**BIC**	**logLik**	**Test**	**L.Ratio**	**p-value**
M3	s(age)	0	3	0	1.000	0.0449	7	-2916.17	-2888.77	1465.08	M3 vs. M5	1.98	0.740
M4	s(pds)	0	3	0	0.681	0.0449	7	-2916.17	-2888.77	1465.08	M4 vs. M5	1.98	0.740
M5	ti(age)	0	3	0	0.561	0.0599	11	-2910.14	-2867.10	1466.07			
	ti(pds)	0	3	0	1.000								
	ti(age, pds)	2.08	2.08	2.12	0.149								
CEN	**Smooth Terms**						**Model Fit**						
	Terms	**edf**	**Ref.df**	**F**	**p-value**	**R2**	**df**	**AIC**	**BIC**	**logLik**	**Test**	**L.Ratio**	**p-value**
M3	s(age)	0.61	3	0.42	0.144	0.0485	7	-3564.77	-3537.38	1789.39	M3 vs. M5	1.89	0.756
M4	s(pds)	0	3	0	0.476	0.0436	7	-3564.36	-3536.97	1789.18	M4 vs. M5	2.30	0.681
M5	ti(age)	0.85	3	1.16	0.034	0.0656	11	-3558.66	-3515.61	1790.33			
	ti(pds)	0	3	0	0.678								
	ti(age, pds)	2.08	2.08	2.25	0.132								
AAA	**Smooth Terms**						**Model Fit**						
	Terms	**edf**	**Ref.df**	**F**	**p-value**	**R2**	**df**	**AIC**	**BIC**	**logLik**	**Test**	**L.Ratio**	**p-value**
M3	s(age)	0.24	3	0.10	0.268	0.0176	7	-3390.84	-3363.45	1702.42	M3 vs. M5	3.90	0.419
M4	s(pds)	0.80	3	0.75	0.079	0.0245	7	-3391.81	-3364.42	1702.91	M4 vs. M5	2.93	0.570
M5	ti(age)	0	3	0	0.620	0.0268	11	-3386.74	-3343.69	1704.37			
	ti(pds)	0	3	0	0.274								
	ti(age, pds)	1	1	3.93	0.048								
ATA	**Smooth Terms**						**Model Fit**						
	Terms	**edf**	**Ref.df**	**F**	**p-value**	**R2**	**df**	**AIC**	**BIC**	**logLik**	**Test**	**L.Ratio**	**p-value**
M3	s(age)	0	3	4.9E-08	0.594	0.0631	7	-3057.41	-3030.02	1535.71	M3 vs. M5	3.65	0.456
M4	s(pds)	0.17	3	0	0.279	0.0640	7	-3057.43	-3030.03	1535.71	M4 vs. M5	3.64	0.458
M5	ti(age)	0	3	0	0.780	0.0731	11	-3053.06	-3010.01	1537.53			
	ti(pds)	0	3	0	0.889								
	ti(age, pds)	1	1	3.64	0.057								
ASTA	**Smooth Terms**						**Model Fit**						
	Terms	**edf**	**Ref.df**	**F**	**p-value**	**R2**	**df**	**AIC**	**BIC**	**logLik**	**Test**	**L.Ratio**	**p-value**
M3	s(age)	0	3	0	0.619	0.0082	7	-3263.98	-3236.58	1638.99	M3 vs. M5	0.06	1.000
M4	s(pds)	0	3	0	0.886	0.0082	7	-3263.98	-3236.58	1638.99	M4 vs. M5	0.06	1.000
M5	ti(age)	0	3	0	0.528	0.0057	11	-3256.04	-3212.99	1639.02			
	ti(pds)	0	3	0	0.699								
	ti(age, pds)	1	1	0.06	0.811								

Notes: In each model, the smooth terms, the estimated degree of freedom (edf), reference degree of freedom (Ref.df), F-score, p-value, and Adjusted R^2 for each model is shown; p-value < 0.0056 bolded (Bonferroni corrected). Between model comparisons include the df, AIC, log-likelihood ratio (L Ratio) and p-values < 0.05 bolded. *For model to converge, 5 knots were chosen instead of 4.

References

Alarcon G, Cservenka A, Rudolph MD, Fair DA, Nagel BJ (2015) Developmental sex differences in resting state functional connectivity of amygdala sub-regions. NeuroImage 115:235-244.

Amaral DG, Price JL (1984) Amygdalo-cortical projections in the monkey (Macaca fascicularis). The Journal of comparative neurology 230:465-496.

Ambroggi F, Ishikawa A, Fields HL, Nicola SM (2008) Basolateral amygdala neurons facilitate rewardseeking behavior by exciting nucleus accumbens neurons. Neuron 59:648-661.

Amunts K, Kedo O, Kindler M, Pieperhoff P, Mohlberg H, Shah NJ, Habel U, Schneider F, Zilles K (2005) Cytoarchitectonic mapping of the human amygdala, hippocampal region and entorhinal cortex: intersubject variability and probability maps. Anatomy and embryology 210:343-352.

Andersen SL, Teicher MH (2008) Stress, sensitive periods and maturational events in adolescent depression. Trends in neurosciences 31:183-191.

Avants B, Anderson C, Grossman M, Gee JC (2007) Spatiotemporal normalization for longitudinal analysis of gray matter atrophy in frontotemporal dementia. Medical image computing and computer-assisted intervention : MICCAI International Conference on Medical Image Computing and Computer-Assisted Intervention 10:303-310.

Avino TA, Barger N, Vargas MV, Carlson EL, Amaral DG, Bauman MD, Schumann CM (2018) Neuron numbers increase in the human amygdala from birth to adulthood, but not in autism. Proceedings of the National Academy of Sciences of the United States of America 115:37103715.

Backhausen LL, Herting MM, Buse J, Roessner V, Smolka MN, Vetter NC (2016) Quality Control of Structural MRI Images Applied Using FreeSurfer-A Hands-On Workflow to Rate Motion Artifacts. Frontiers in neuroscience 10:558.

Barbas H, De Olmos J (1990) Projections from the amygdala to basoventral and mediodorsal prefrontal regions in the rhesus monkey. The Journal of comparative neurology 300:549-571.

Baxter MG, Murray EA (2002) The amygdala and reward. Nature reviews Neuroscience 3:563-573.

Berenbaum SA, Beltz AM, Corley R (2015) The importance of puberty for adolescent development: conceptualization and measurement. Advances in child development and behavior 48:53-92.

Bernier PJ, Bedard A, Vinet J, Levesque M, Parent A (2002) Newly generated neurons in the amygdala and adjoining cortex of adult primates. Proceedings of the National Academy of Sciences of the United States of America 99:11464-11469.

Bonferroni CE (1936) Teoria statistica delle classi e calcolo delle probabilita. Pubblicazioni del R Istituto Superiore di Sceinze Economiche e Commerciali di Firenze 8:3-62.

Bramen JE, Hranilovich JA, Dahl RE, Forbes EE, Chen J, Toga AW, Dinov ID, Worthman CM, Sowell ER (2011) Puberty influences medial temporal lobe and cortical gray matter maturation differently in boys than girls matched for sexual maturity. Cerebral cortex (New York, NY : 1991) 21:636-646.

Bzdok D, Laird AR, Zilles K, Fox PT, Eickhoff SB (2013) An investigation of the structural, connectional, and functional subspecialization in the human amygdala. Human brain mapping 34:3247-3266.

Chaplin TM, Aldao A (2013) Gender differences in emotion expression in children: a meta-analytic review. Psychological bulletin 139:735-765.

Cservenka A, Stroup ML, Etkin A, Nagel BJ (2015) The effects of age, sex, and hormones on emotional conflict-related brain response during adolescence. Brain and cognition 99:135-150.

Cunningham MG, Bhattacharyya S, Benes FM (2002) Amygdalo-cortical sprouting continues into early adulthood: implications for the development of normal and abnormal function during adolescence. The Journal of comparative neurology 453:116-130.

deCampo DM, Fudge JL (2012) Where and what is the paralaminar nucleus? A review on a unique and frequently overlooked area of the primate amygdala. Neuroscience and biobehavioral reviews 36:520-535.

deCampo DM, Fudge JL (2013) Amygdala projections to the lateral bed nucleus of the stria terminalis in the macaque: comparison with ventral striatal afferents. The Journal of comparative neurology 521:3191-3216.

Dorn LD (2006) Measuring puberty. J Adolesc Health 39:625-626.

Gabard-Durnam LJ, Flannery J, Goff B, Gee DG, Humphreys KL, Telzer E, Hare T, Tottenham N (2014) The development of human amygdala functional connectivity at rest from 4 to 23 years: a cross-sectional study. NeuroImage 95:193-207.

Ghashghaei HT, Barbas H (2002) Pathways for emotion: interactions of prefrontal and anterior temporal pathways in the amygdala of the rhesus monkey. Neuroscience 115:1261-1279.

Giedd JN, Vaituzis AC, Hamburger SD, Lange N, Rajapakse JC, Kaysen D, Vauss YC, Rapoport JL (1996) Quantitative MRI of the temporal lobe, amygdala, and hippocampus in normal human development: ages 4-18 years. The Journal of comparative neurology 366:223-230.

Goddings AL, Mills KL, Clasen LS, Giedd JN, Viner RM, Blakemore SJ (2014) The influence of puberty on subcortical brain development. NeuroImage 88:242-251.

Hariri AR, Tessitore A, Mattay VS, Fera F, Weinberger DR (2002) The amygdala response to emotional stimuli: a comparison of faces and scenes. NeuroImage 17:317-323.

Herting MM, Gautam P, Spielberg JM, Kan E, Dahl RE, Sowell ER (2014) The role of testosterone and estradiol in brain volume changes across adolescence: a longitudinal structural MRI study. Human brain mapping 35:5633-5645.

Herting MM, Johnson C, Mills KL, Vijayakumar N, Dennison M, Liu C, Goddings AL, Dahl RE, Sowell ER, Whittle S, Allen NB, Tamnes CK (2018) Development of subcortical volumes across adolescence in males and females: A multisample study of longitudinal changes. NeuroImage 172:194-205.

Janak PH, Tye KM (2015) From circuits to behaviour in the amygdala. Nature 517:284-292.

Jenkinson M, Beckmann CF, Behrens TE, Woolrich MW, Smith SM (2012) FSL. NeuroImage 62:782790.

Killcross S, Robbins TW, Everitt BJ (1997) Different types of fear-conditioned behaviour mediated by separate nuclei within amygdala. Nature 388:377-380.

Krettek JE, Price JL (1978) A description of the amygdaloid complex in the rat and cat with observations on intra-amygdaloid axonal connections. The Journal of comparative neurology 178:255-280.

McDonald AJ, Jackson TR (1987) Amygdaloid connections with posterior insular and temporal cortical areas in the rat. The Journal of comparative neurology 262:59-77.

Meyer-Lindenberg A, Hariri AR, Munoz KE, Mervis CB, Mattay VS, Morris CA, Berman KF (2005) Neural correlates of genetically abnormal social cognition in Williams syndrome. Nature neuroscience 8:991-993.

Morales AM, Jones SA, Ehlers A, Lavine JB, Nagel BJ (2018) Ventral striatal response during decision making involving risk and reward is associated with future binge drinking in adolescents. Neuropsychopharmacology : official publication of the American College of Neuropsychopharmacology 43:1884-1890.

Must A, Anderson SE (2006) Body mass index in children and adolescents: considerations for population-based applications. International journal of obesity (2005) 30:590-594.

Pauli WM, Nili AN, Tyszka JM (2018) A high-resolution probabilistic in vivo atlas of human subcortical brain nuclei. Scientific data 5:180063.

Petersen AC, Crockett L, Richards M, Boxer A (1988) A self-report measure of pubertal status: Reliability, validity, and initial norms. Journal of youth and adolescence 17:117-133.

Phillips RG, LeDoux JE (1992) Differential contribution of amygdala and hippocampus to cued and contextual fear conditioning. Behavioral neuroscience 106:274-285.

Pitkanen A, Amaral DG (1998) Organization of the intrinsic connections of the monkey amygdaloid complex: projections originating in the lateral nucleus. The Journal of comparative neurology 398:431-458.

Raznahan A, Lerch JP, Lee N, Greenstein D, Wallace GL, Stockman M, Clasen L, Shaw PW, Giedd JN (2011) Patterns of coordinated anatomical change in human cortical development: a longitudinal neuroimaging study of maturational coupling. Neuron 72:873-884.

Rollins BL, King BM (2000) Amygdala-lesion obesity: what is the role of the various amygdaloid nuclei? American journal of physiology Regulatory, integrative and comparative physiology 279:R13481356.

Sah P, Faber ES, Lopez De Armentia M, Power J (2003) The amygdaloid complex: anatomy and physiology. Physiological reviews 83:803-834.

Sananes CB, Davis M (1992) N-methyl-D-aspartate lesions of the lateral and basolateral nuclei of the amygdala block fear-potentiated startle and shock sensitization of startle. Behavioral neuroscience 106:72-80.

Saygin ZM, Kliemann D, Iglesias JE, van der Kouwe AJW, Boyd E, Reuter M, Stevens A, Van Leemput K, McKee A, Frosch MP, Fischl B, Augustinack JC (2017) High-resolution magnetic resonance imaging reveals nuclei of the human amygdala: manual segmentation to automatic atlas. NeuroImage 155:370-382.

Scheuer H, Alarcon G, Demeter DV, Earl E, Fair DA, Nagel BJ (2017) Reduced fronto-amygdalar connectivity in adolescence is associated with increased depression symptoms over time. Psychiatry research Neuroimaging 266:35-41.

Schoenbaum G, Chiba AA, Gallagher M (1999) Neural encoding in orbitofrontal cortex and basolateral amygdala during olfactory discrimination learning. The Journal of neuroscience : the official journal of the Society for Neuroscience 19:1876-1884.

Smith SM, Jenkinson M, Woolrich MW, Beckmann CF, Behrens TE, Johansen-Berg H, Bannister PR, De Luca M, Drobnjak I, Flitney DE, Niazy RK, Saunders J, Vickers J, Zhang Y, De Stefano N, Brady JM, Matthews PM (2004) Advances in functional and structural MR image analysis and implementation as FSL. NeuroImage 23 Suppl 1:S208-219.

Solano-Castiella E, Schafer A, Reimer E, Turke E, Proger T, Lohmann G, Trampel R, Turner R (2011) Parcellation of human amygdala in vivo using ultra high field structural MRI. NeuroImage 58:741-748.

Stan AD, Ghose S, Gao XM, Roberts RC, Lewis-Amezcua K, Hatanpaa KJ, Tamminga CA (2006) Human postmortem tissue: what quality markers matter? Brain research 1123:1-11.

Tosevski J, Malikovic A, Mojsilovic-Petrovic J, Lackovic V, Peulic M, Sazdanovic P, Alexopulos C (2002) Types of neurons and some dendritic patterns of basolateral amygdala in humans--a golgi study. Annals of anatomy = Anatomischer Anzeiger : official organ of the Anatomische Gesellschaft 184:93-103.

Tottenham N, Gabard-Durnam LJ (2017) The developing amygdala: a student of the world and a teacher of the cortex. Current opinion in psychology 17:55-60.

Tyszka JM, Pauli WM (2016) In vivo delineation of subdivisions of the human amygdaloid complex in a high-resolution group template. Human brain mapping 37:3979-3998.

Wan FJ, Swerdlow NR (1997) The basolateral amygdala regulates sensorimotor gating of acoustic startle in the rat. Neuroscience 76:715-724.

Wierenga L, Langen M, Ambrosino S, van Dijk S, Oranje B, Durston S (2014) Typical development of basal ganglia, hippocampus, amygdala and cerebellum from age 7 to 24. NeuroImage 96:67-72.

Wierenga LM, Bos MGN, Schreuders E, Vd Kamp F, Peper JS, Tamnes CK, Crone EA (2018) Unraveling age, puberty and testosterone effects on subcortical brain development across adolescence. Psychoneuroendocrinology 91:105-114.

Woolrich MW, Jbabdi S, Patenaude B, Chappell M, Makni S, Behrens T, Beckmann C, Jenkinson M, Smith SM (2009) Bayesian analysis of neuroimaging data in FSL. NeuroImage 45:S173-186.